*Journal of Biomolecular NMR*, **12:** 209–222, 1998.
*KLUWER/ESCOM*



# Hydrogen bonding geometry of a protein-bound carbohydrate from water exchange-mediated cross-relaxation

Eric W. Sayers[a], Jeanne L. Weaver[b] & James H. Prestegard[b,*]
[a]*Department of Pharmacology, Yale University, 333 Cedar Street, New Haven, CT 06510, U.S.A.*
[b]*Department of Chemistry, Yale University, P.O. Box 208107, New Haven, CT 06520-2817, U.S.A.*

Received 19 September 1997; Accepted 1 December 1997

*Key words:* $^{13}$C-edited NMR, $^{13}$C-labeled carbohydrate, hydroxyl protons, mannose binding protein

**Abstract**

We present heteronuclear two-dimensional methods for the analysis of the geometry of exchangeable protons on a protein-bound carbohydrate. By using a water-selective NOESY-HSQC, we observed cross-relaxation between carbohydrate hydroxyl protons and non-exchangeable ring protons in the complex of [$^{13}C_6$]-α-methyl-D-mannopyranoside with recombinant rat mannose binding protein. Using a simple kinetic model, we were able to explain the differences in the initial slopes of the resulting cross-relaxation buildup curves in terms of the geometry of the hydroxyl protons in the bound state. The hydroxyl rotamers consistent with our cross-relaxation data fit very well with predictions based on the crystal structure of MBP bound to a mannose-rich oligosaccharide. These methods should be applicable to other systems where both ligand exchange and water exchange are fast relative to the rate of cross-relaxation.

## Introduction

The interactions between carbohydrates and proteins are increasingly recognized as the basis for a number of important processes in biology, including cell–cell adhesion, cell recognition, and host defense (Lasky, 1992; Bevilacqua, 1993; Opdenakker et al., 1993). Because of their importance, the structural details of protein-carbohydrate complexes have been explored using both X-ray crystallography and NMR, and various structural models have been proposed to explain the specificity of the interactions. Many of these models include a large network of hydrogen bonds connecting hydroxyl groups of the sugar to proton donor and acceptor residues of the protein (Quiocho, 1989). Such networks are thought to underlie in large part both the specificity and the energetic stability of these complexes. However, hydroxyl protons are not easy targets for structural studies, either for the X-ray crystallographer or the NMR spectroscopist. The low electron density around hydroxyl protons makes it difficult to position them directly on the basis of X-ray diffraction data. The situation is little better in NMR spectroscopy, since the high rates of exchange of hydroxyl protons with solvent protons in aqueous solution result in the hydroxyl lines averaging into the large solvent resonance; thus there is no direct spectral resolution of different hydroxyl sites. NMR does, however, offer the possibility of indirect detection through better resolved sites. It was our objective to use this indirect approach in designing NMR experiments which could yield structural information regarding hydroxyl protons on a protein-complexed carbohydrate in aqueous solution.

Over the past several years a variety of NMR techniques have been proposed for the study of carbohydrate hydroxyl protons. One of the oldest strategies is to dissolve the carbohydrate in an aprotic solvent such as DMSO in which sharp, well-resolved lines for hydroxyl protons can be directly observed, a method first introduced over thirty years ago (Casu et al., 1966). However, such solvents cannot mimic protein hydrogen bonding environments. More recently, other investigators have used low temperature as a means

* To whom correspondence should be addressed.

of inhibiting hydroxyl exchange in aqueous solvents. This generally requires temperatures well below 0 °C, and so it is necessary to include a substantial amount ($\geq$ 15% v/v) of a second solvent, such as acetone, to depress the freezing point (Poppe and van Halbeek, 1991; Adams and Lerner, 1992, 1994). Even more recently, hydroxyl resonances were successfully observed in supercooled, pure aqueous solutions, thus eliminating the need for such second solvents (Poppe and van Halbeek, 1994). While these methods have proven to be very useful for the study of free carbohydrates, the conditions of these experiments are far from physiological and thus may be poor choices for studies involving biologically active proteins.

Here we present an approach in which the water magnetization is used to selectively perturb the hydroxyl protons of a $^{13}$C-labeled carbohydrate ligand complexed to an unlabeled protein under physiological conditions. The combined use of selective water excitation and $^{13}$C filtering allows data specific to water-exchangeable protons of the bound carbohydrate ligand to be obtained via cross-relaxation to the non-exchangeable, $^{13}$C-coupled ring protons. This approach closely parallels several well-established methods for studying amide exchange in $^{15}$N-labeled proteins (Grzesiek and Bax, 1993; Kriwacki et al., 1993; Mori et al., 1996), as well as transfer NOE methods for studying ligands in fast exchange between free and bound states (Clore and Gronenborn, 1983; Campbell and Sykes, 1993). The proposed pathway of exchange-mediated cross-relaxation has been long recognized as a possible mechanism of magnetization transfer in macromolecules (Liepinsh and Otting, 1996). We merely extend the idea to magnetization transfers on a ligand transiently associated with a protein.

We illustrate this approach by using a recombinant fragment of rat mannose binding protein. Mannose binding protein (MBP) is a member of the collectin family of mammalian lectins, and is found in the liver and blood. It serves as a host defense molecule by binding to surface carbohydrates of an invading bacterium and once bound, activating the complement cascade which results in the destruction of the bacterium (Hoppe and Reid, 1994a, b). MBP, a homo-oligomeric protein, binds to these carbohydrates through its several C-terminal calcium-dependent carbohydrate recognition domains (CRD). Each CRD binds one equivalent from a small selection of monosaccharides which includes D-mannose and D-glucose (Lee et al., 1991; Iobst et al., 1994).

A 155 amino acid fragment of rat serum MBP, including the CRD, has been overexpressed in *E. coli*, and this 17.8 kDa fragment has been shown to retain carbohydrate affinity (Weis et al., 1991a). The fragment forms homotrimers at concentrations relevant for NMR studies, giving the system an effective mass of 53.4 kDa. The fragment can be reduced in size to 12.5 kDa by proteolysis using subtilisin. The proteolysis product forms a homodimer, and the crystal structure of the dimer with and without a bound mannose-rich oligosaccharide ligand was solved a few years ago (Weis et al., 1991b, 1992). More recently, the crystal structures of both the rat and human trimeric proteins have been solved (Chang et al., 1994; Sheriff et al., 1994; Weis and Drickamer, 1994). Here, we present data acquired on the complex between a model ligand, [$^{13}C_6$]-α-methyl-D-mannopyranoside, and the 53.4 kDa trimeric fragment of MBP.

## Materials and methods

*Synthesis of [$^{13}C_6$]-α-methyl-D-mannopyranoside*

[$^{13}C_6$]-α-methyl-D-mannopyranoside was synthesized from [$^{13}C_6$]-D-glucose (Isotec, Inc., Miamisburg, OH, U-[$^{13}C_6$], 81.2%) using a slight modification of a previous method (Hare et al., 1993). Briefly, following the preparation of the [$^{13}C_6$]-tri-*O*-acetyl-D-glucal, 143 mg (0.525 mmol) was dissolved in 3 ml benzene. Methanol (143 μl, 3.53 mmol) and boron trifluoride diethyl etherate (35 μl, 0.28 mmol) were added, and the reaction was stirred for 1 h at room temperature (Ferrier and Prasad, 1968). The resulting product, [$^{13}C_6$]-α-methyl-2,3-dideoxy-4,6-di-*O*-acetyl-D-glucopyranoside, was purified by flash chromatography on silica with a solvent of 1:3 ethylacetate:hexane. The purified 2,3-dideoxy product was then oxidized to the corresponding glycol using osmium tetroxide and sodium bisulfite, and then deacetylated as previously described (Hare et al., 1993) to yield [$^{13}C_6$]-α-methyl-D-mannopyranoside.

*Expression of mannose binding protein*

Plasmid pINIIIompA2 containing the 3′ portion of the rat serum MBP cDNA (Drickamer, 1989) was used to transform *Escherichia coli* strain JA221 cells, and the growth, expression, and purification of the MBP CRD were performed as previously described (Weis et al., 1991a). Briefly, after harvesting cells and lysis by sonication, the insoluble pellet from a 10 000 × g centrifugation was solubilized in 6M guanidine hydrochloride,

clarified at 100 000× g, and diluted with 4 volumes of loading buffer (1.25 M NaCl, 25 mM Tris-Cl pH 7.8, 25 mM $CaCl_2$). After extensive dialysis of this extract against loading buffer, the dialysate was applied to a 10-ml mannose-Sepharose column (Fornstedt and Porath, 1975). Purified MBP was eluted with loading buffer containing 2.5 mM EDTA instead of $CaCl_2$, and column fractions containing protein were analyzed by SDS-PAGE.

*NMR sample preparation*

Fractions from the mannose-Sepharose column containing pure protein were pooled and dialyzed three times against 100 volumes of 25 mM Tris-Cl pH 7.8 to remove salt. The dialysate was lyophilized and redissolved in 1 ml $ddH_2O$ and applied to a PD-10 gel filtration column (Pharmacia Biotech, Piscataway, NJ) equilibrated with $ddH_2O$ to remove protonated Tris-Cl. The final lyophilate was dissolved in the desired volume (0.2–0.5 ml) of 10 mM $d^{11}$-Tris-Cl pH 7.8 (Isotec, Inc.) containing 20 mM $CaCl_2$ and 10% $D_2O$, and then added to the desired amount of dried mannoside.

*NMR spectroscopy*

All spectra were acquired on a GE Omega spectrometer operating at 500 MHz and equipped with a Bruker triple-resonance triple-axis gradient probe and an S-17 gradient accessory. After collection, data were processed using FELIX software (version 2.3 or 95.0, Biosym Technologies, San Diego, CA, USA). All chemical shifts are reported relative to internal DSS as previously outlined (Wishart et al., 1995).

Proton chemical shift assignments for α-methylmannoside were obtained from the literature (Hounsell, 1995) and confirmed by a 2D DQF-COSY spectrum (data not shown). Carbon chemical shifts were obtained from a 2D $^1$H-$^{13}$C HSQC spectrum.

HSQC spectra were recorded using pulsed field gradients to accomplish coherence selection (Davis et al., 1992; Tolman et al., 1992). The proton carrier was placed on the water resonance and 1024 complex points were acquired with a spectral width of 5000 Hz. The carbon carrier was placed at 82.57 ppm and 128 complex points were acquired with a spectral width of 7500 Hz. Twelve scans were collected for each $t_1$ increment, and each direct dimension FID was apodized using a Kaiser window prior to Fourier transformation. Indirect FIDs were zero-filled to 512 points and apodized using a squared sinebell window prior to Fourier transformation, yielding a 1024 × 512 matrix.

Carbon-13 filtered NOESY spectra were acquired using a pulse sequence based largely on a published 3D NOESY-HSQC experiment (Muhandiram et al., 1993) which was modified by adding gradient coherence selection to the HSQC as well as a water selective 90° pulse toward the end of the mixing time which resulted in water being restored to the positive z axis at the beginning of subsequent data acquisition. The experiment was acquired by incrementing only the proton evolution time, which yielded essentially a 2D $^{13}$C-filtered $^1$H-$^1$H NOESY spectrum. The proton and carbon carriers were placed on the water resonance and at 82.57 ppm, respectively. Sixty-four scans were acquired for each of 256 complex $t_1$ points. The data size of the direct dimension was 1024 complex points, and the spectral width of each dimension was 5000 Hz. The indirect dimension was zero-filled to 1024 points, and apodized using a skewed squared sinebell prior to Fourier transformation, yielding a 1024 × 1024 matrix.

Water-selective NOESY-HSQC experiments were acquired using the sequence depicted in Figure 3 and described in the Results section. For one-dimensional versions of this experiment, 2880 scans of 1024 complex points each were collected using a spectral width of 5000 Hz. The proton and carbon carriers were placed on the water resonance and at 82.57 ppm, respectively. For two-dimensional versions of this experiment, the carbon carrier was moved to 67.57 ppm and 208 scans were collected for each of 16 complex $t_1$ points. The data size of the direct dimension was 1024 complex points, and the spectral widths in the direct and indirect dimensions were 5000 Hz and 2500 Hz, respectively.

## Results

*Characterization of MBP-ligand exchange*

The binding behavior of labeled α-methylmannoside to MBP was initially characterized by performing 2D $^1$H-$^{13}$C HSQC experiments on the sugar in the absence and presence of a 1:1 molar ratio of MBP monomer. Two representative spectra are shown in Figure 1. Significant broadening of the sugar resonances is observed upon addition of MBP at all sugar sites, with an average broadening of 15 Hz in the proton dimension at 35 °C. The expected broadening of $^{13}$C-attached protons bound to MBP is on the order of 60 Hz, assuming that MBP is a spherical trimer with a rotational

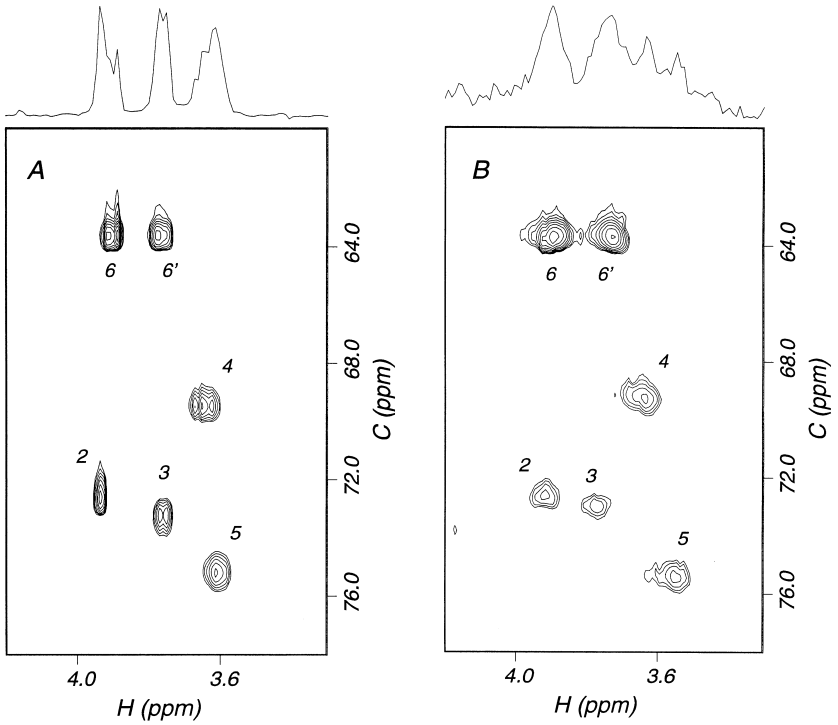


*Figure 1.* 2D HSQC spectra acquired at 35 °C of the mannoside in the absence (A) and presence (B) of MBP. The concentration of mannoside was 6 mM in the sample without MBP, and 1.4 mM in the presence of 1.8 mM MBP monomers. The sums of all F1 slices of both spectra are displayed as one-dimensional projections above each map. Peaks are labeled by the ring proton/ring carbon spin pairs.

correlation time of 25 ns (Cavanagh et al., 1996). Based on the known dissociation constant, 2.8 mM (Iobst et al., 1994), approximately 30% of the mannoside should have been bound to MBP. Thus, the observed broadening is consistent with broadening expected for fast exchange of the ligand between bound and free forms ($\sim$ 20 Hz).

In addition, it is apparent from the spectra in Figure 1 that the proton chemical shifts of the sugar were slightly perturbed upon addition of MBP. The chemical shifts of three of the six labeled carbons, C3, C4, and C5, were also measurably perturbed upon addition of MBP. These chemical shift changes are summarized in Table 1. Such shifts, combined with the lack of any new resonances that might represent a bound sugar species, are also consistent with the free and bound sugar species being in fast exchange on the NMR timescale. An examination of the temperature dependence of the proton line widths showed that these lines narrow substantially with increasing temperature, further confirming the occurrence of fast exchange.

*Table 1.* Chemical shift changes at 35 °C of mannoside ring protons upon binding to MBP ($\sim$ 30% bound)

| | $^{1}$H shifts (ppm) | | | $^{13}$C shifts (ppm) | | |
|---|---|---|---|---|---|---|
| Site | −MBP | +MBP | Δ | −MBP | +MBP | Δ |
| 1 | 4.76 | 4.73 | −0.03 | 103.5 | 103.5 | 0.0 |
| 2 | 3.94 | 3.92 | −0.02 | 72.7 | 72.6 | −0.1 |
| 3 | 3.76 | 3.78 | 0.02 | 73.3 | 73.0 | −0.3 |
| 4 | 3.65 | 3.64 | −0.01 | 69.5 | 69.3 | −0.2 |
| 5 | 3.62 | 3.56 | −0.06 | 75.2 | 75.4 | 0.2 |
| 6 | 3.90 | 3.90 | 0.00 | 63.6 | 63.7 | 0.1 |
| 6′ | 3.77 | 3.73 | −0.04 | – | – | – |

*Observation of exchange-mediated cross-relaxation*

To establish cross-relaxation connectivities important to our ligand, we first employed an experiment that would broadly detect all sources of cross-relaxation to non-exchanging $^{13}$C-bound protons. This was achieved by acquiring a 2D $^{13}$C-filtered $^{1}$H-$^{1}$H NOESY spectrum. A portion of a representative spectrum recorded with a mixing time of 50 ms is shown in Figure 2. Clearly visible is the $^{13}$C-filtered pro-

ton diagonal representing ring proton magnetization of the mannoside. There are some small distortions of the positions of peaks on the diagonal because the mannoside preparation contained a minor contaminant (∼ 2%). Because the contaminant does not bind to MBP, the corresponding peaks remain sharp and contribute anomalously to the diagonal intensity. Near the diagonal are several broad cross peaks, corresponding to intramolecular cross-relaxation between non-exchangeable protons of the mannoside. These are dominated by the bound species and accurately reflect bound mannose chemical shifts. The most pronounced feature is the strong connection between the water resonance at 4.75 ppm and several non-exchangeable sugar protons. These cross peaks must arise from a transfer of magnetization that originated either on water protons, protons in fast exchange with water, or protons whose chemical shifts are degenerate with that of water. Two other features of these cross peaks are worth noting: first, all of these cross peaks have the same phase as the diagonal peaks, indicating that cross-relaxation occurred on a slowly tumbling species; second, while cross-relaxation must play some role in the genesis of these peaks, as it does in the intrasugar peaks, the sheer intensity of these cross peaks relative to the diagonal peaks is anomalous. Both the origin and intensity of these peaks, as we shall discuss below, can be explained by a combination of cross-relaxation and exchange coupling to an intense bulk water resonance.

While the experimental results depicted in Figure 2 show several strong cross peaks at the frequency band of the water resonance, the results are difficult to interpret in terms of connections to specific mannose protons. The inherent short $T_2$ of the bound sugar resonances, combined with some exchange broadening at 25 °C yielded broad lines with poor resolution. This made assignment of these cross peaks very difficult. Thus, we proceeded with a more efficient water-selective experiment in which the better resolved $^{13}$C shifts were encoded in the indirect dimension.

*Assignment of exchange/cross-relaxation cross peaks*

Since we are interested only in the cross peaks occurring at the frequency of water in F1, little is lost in selectively inverting water instead of frequency resolving water in the indirect dimension. We therefore move the $t_1$ evolution time to the carbon dimension where the carbon chemical shift can be used to aid in the assignments of these cross peaks. Such an experimental approach has been used previously in the study

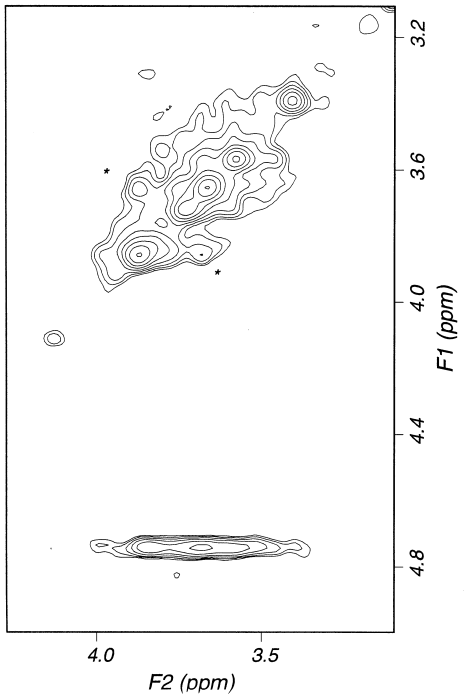


*Figure 2.* 2D $^{13}$C filtered NOESY spectrum acquired with a mixing time of 50 ms. The spectrum was collected at 25 °C on a sample containing 1.8 mM MBP monomer and 1.4 mM mannoside. The contours are geometric with a factor of 1.4 between adjacent levels. Asterisks indicate NOE cross peaks between H6 and H6′.

of water-amide exchange in protein systems (Grzesiek and Bax, 1993; Kriwacki et al., 1993; Andrec et al., 1995; Mori et al., 1996). The pulse sequence used to this end is displayed in Figure 3. The experiment begins with a selective inversion pulse on water, followed immediately by a mixing time during which exchange and cross-relaxation take place. Gradients G1 and G2 at the beginning and end of this period serve to prevent radiation damping of the water magnetization. This period is followed by a conventional gradient-selected HSQC sequence, which selectively passes only that proton magnetization that resides on protons coupled to $^{13}$C nuclei at the end of the mixing time. In this sequence, gradients G4 and G6 accomplish the selection of the desired coherence pathway, while gradients G3 and G5 serve to suppress water during periods in which the desired magnetization is along the z axis in two spin order. The experiment is performed as a difference experiment between scans with and without the initial water-selective pulse. An enhanced version of the HSQC was not used but could be easily incorporated.

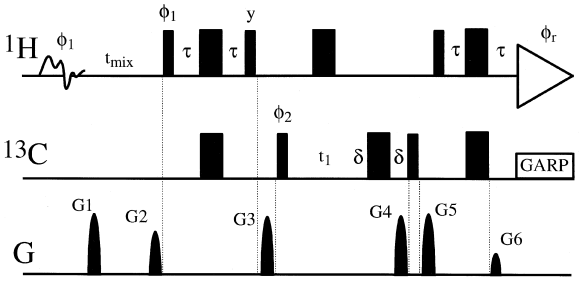


*Figure 3.* The water-selective NOESY-HSQC experiment. Narrow and wide pulses represent flip angles of 90° and 180°, respectively. All $^{1}$H and $^{13}$C hard pulses were applied at respective fields of 32.9 kHz and 23.8 kHz for the one-dimensional experiment, and 39.8 kHz and 22.7 kHz for the two-dimensional experiment. The $^{1}$H 180° pulse in the middle of the $t_1$ period was a composite pulse (90°y, 180°x, 90°y). The initial water-selective inversion pulse used was that developed by Shinnar and LeRoux (LeRoux, 1988; Shinnar et al., 1989; John et al., 1992), and was applied for 50 ms (80 Hz field at peak amplitude). Using this pulse, approximately 80% of the water magnetization was inverted compared to that excited by a 90° hard pulse. Carbon decoupling during acquisition was achieved using GARP (Shaka et al., 1985) applied using a 5 kHz field. Values for delays were as follows: $t_{mix} = 30 - 150$ ms, $\tau = 1.56$ ms, $\delta = 1.05$ ms, relaxation delay = 2.0 s. In the one-dimensional experiment, the $t_1$ evolution period was set to a constant duration of 16 μs. The duration and strengths of the gradient pulses were as follows: G1 = 30 G/cm, 1.0 ms; G2 = 15 G/cm, 1.0 ms; G3 = G4 = G5 = 30 G/cm, 1.0 ms; G6 = 7.5 G/cm, 1.0 ms. All gradients were applied as shaped sinusoids. A ring down delay of at least 50 μs was inserted after each gradient pulse to prevent signal loss from eddy currents. The phase cycle used was the following: $\phi_1 = (x, x, -x, -x)$, $\phi_2 = (x, -x)$, Rec. $= (x, -x, -x, x)$. In addition, alternate sets of 8 transients each were collected with the power of the selective pulse either off or on, and the phase of the receiver was inverted for the second set. Before acquiring the difference experiment, a spectrum acquired without the selective pulse was phased absorptive, allowing the phase of the cross-relaxation peaks to be determined from the order of the subtraction. Quadrature detection in $t_1$ in the two-dimensional experiment was achieved by collecting two data sets at each value of t1, and by inverting the sign of gradient G6 for the second set (Tolman et al., 1992).

A potential problem in the use of the proposed experiment is that spins other than water may be inverted by the selective pulse. One possible candidate for such unwanted inversion is the anomeric proton of the mannoside, which resonates within 0.02 ppm of water (see Table 1). To eliminate the possibility that inversion of the anomeric proton by the water-selective pulses resulted in a significant contribution to the observed cross peaks, the sample was analyzed using a modified version of a closely related experiment (Grzesiek and Bax, 1993) which contains an initial pulse sequence element designed to destroy the magnetization of any proton that is both directly attached to a $^{13}$C and is excited by the initial selective pulse. The remainder of the experiment of Grzesiek and Bax is conceptually the same as that proposed in Figure 3, with the exception that it contains $^{15}$N- and $^{13}$C-carbonyl pulses used in the study of $^{15}$N/$^{13}$C labeled proteins. We removed these pulses, and the results using this modified sequence gave signal buildup rates that were largely unchanged from those produced by the experiment in Figure 3.

The experiment in Figure 3 was initially run with a fixed value of $t_1$ to produce an efficiently collected 1D version of Figure 2 which was used to monitor the rate of magnetization transfer. Notably, these spectra contained no signals at the chemical shifts of sharp contaminant peaks, and moreover, when the experiment was performed on a sample of the free mannoside alone, the spectra contained no signals whatsoever, indicating that MBP is required for the observed cross-relaxation to occur (data not shown). However, the overlap in these spectra remained severe and prevented any more detailed analysis of the kinetics at individual sites on the mannoside. To resolve these sites, we repeated the series of experiments using the same pulse sequence, but this time collected an HSQC for each mixing time, thus generating a series of 2D maps in which the exchange/cross-relaxation peaks were spread out along a $^{13}$C dimension. A portion of one of these maps, corresponding to $t_{mix} =$ 90 ms, is displayed in Figure 4 alongside a conventional HSQC. The water-selective 2D spectrum shows peaks in positions that are essentially identical to the conventional HSQC; however, it is apparent that the relative intensities of the peaks are quite different in the two spectra. Most obvious is the marked reduction of the peak for position 5, but it is clear that the peaks for the two exocyclic positions, 6 and 6′, are also reduced significantly. These observations are more clearly shown in Figure 5, where the volumes of the peaks in the water-selective experiments, normalized against the volumes of HSQC peaks for the mannoside in the absence of water-mediated cross-relaxation, have been plotted versus mixing time. The six non-exchangeable sites on the mannoside for which data could be measured cluster into three groups based on their relative rates of signal buildup: protons 2, 3, and 4, having relatively fast buildup rates; the two exocyclic protons 6 and 6′, having moderate buildup rates; and proton 5, having a significantly slower buildup rate. The anomeric proton was not analyzed because of the proximity of its chemical shift to that of water.

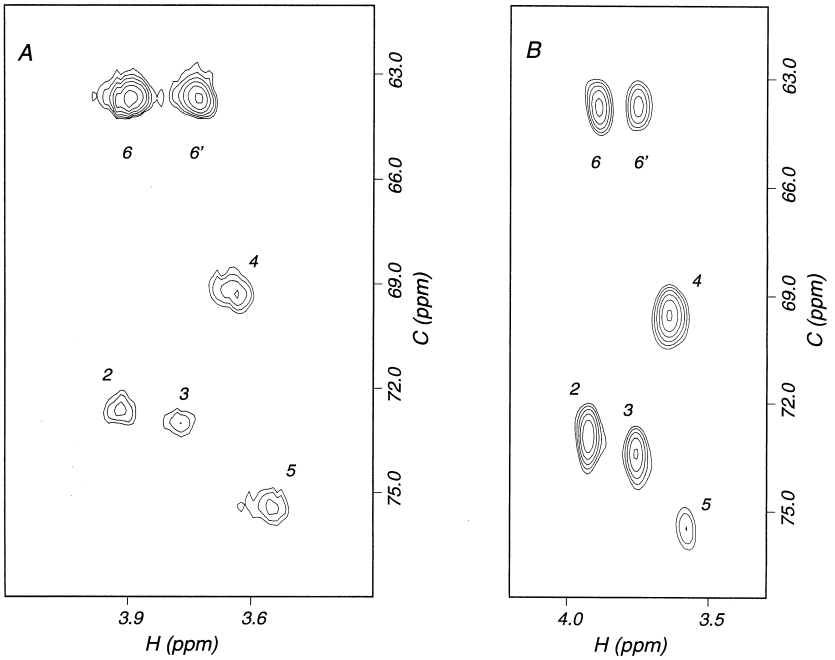


*Figure 4.* 2D water-selective NOESY-HSQC. Spectrum A was acquired using a standard gradient-selected HSQC experiment on a sample containing 1.8 mM MBP monomer and 1.4 mM mannoside, and is shown for comparison. Spectrum B was acquired using the pulse sequence of Figure 3 on a sample containing 1.0 mM MBP monomer and 1.2 mM mannoside. The value of $t_{mix}$ was set to 90 ms. Both spectra were acquired at 35 °C, and peaks are labeled by the ring proton/ring carbon spin pairs.

## Discussion

### *Development of a kinetic model*

Interpretation of the experimental observations presented in Figures 2 and 5 requires answers to two questions: first, why are the water-selective cross-relaxation buildup rates different for the various mannoside ring protons; and second, why are the water cross peaks enhanced relative to the intrasugar cross peaks. Both depend on the details of how water magnetization is transferred to the mannoside ring protons. One can envision at least three pathways for this magnetization transfer. Magnetization could transfer directly from a proton on water to non-exchangeable ligand protons; the transfer could be mediated by protons on the protein that are either in fast exchange with water (e.g. hydroxyl or amide protons) or degenerate with water (e.g. alpha protons); or the transfer of magnetization could be mediated by sugar hydroxyl protons. According to the model based on the crystal structure, the MBP binding site lies on the surface of the protein, where the mannoside might be directed toward highly mobile solvent molecules (Weis et al., 1992). However, in order for a solvent molecule to produce cross-relaxation peaks having the phase observed in the present study, these water molecules must be immobilized with correlation times longer than the reciprocal of the Larmor precession frequency (500 MHz), or greater than 2 ns. Previous investigators studying small proteins, such as the trypsin inhibitor, BPTI, showed that this limit corresponds to a lifetime for a surface water of approximately 500 ps, and failed to find evidence of any surface water molecules with lifetimes longer than this even at 4 °C (Otting et al., 1991). Given that our experiments were conducted at temperatures of 25 °C or higher, the possibility of such long-lived surface waters is quite low. Hence we discount the first mechanism. With respect to the possibility that the transfers could be mediated by protein protons, the X-ray data show that the MBP binding site is proton poor, being composed mostly of the oxygen and nitrogen ligands of the coordinated calcium. Indeed, the alpha protons nearest to the ligand are over 5 Å away. The only exchangeable protons within this distance of the mannoside are the side chain amide protons of Asn 187 and Asn 205. However, these protons are unlikely to be exchanging with water sufficiently fast to be averaged with the water resonance, and thus, inverted by the initial selective pulse. We are thus left with the third possibility, which is that

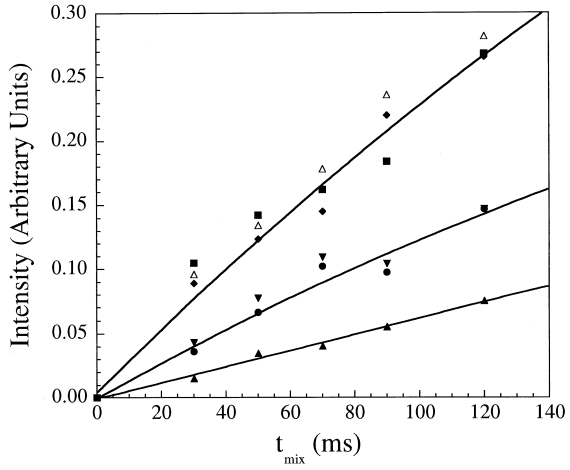


*Figure 5.* Integrated intensities of cross peaks from a series of 2D spectra acquired at 35 °C using the pulse sequence in Figure 3. Peak integrals were normalized relative to those of an HSQC spectrum of the free mannoside. Labels correspond to individual ring proton/ring carbon spin pairs, as follows: △= H2, ■ = H3, ♦ = H4, ▲ = H5, ▼ = H6, ● = H6′. Solid lines are the best exponentials through data points at sites H4, H5, and H6′.

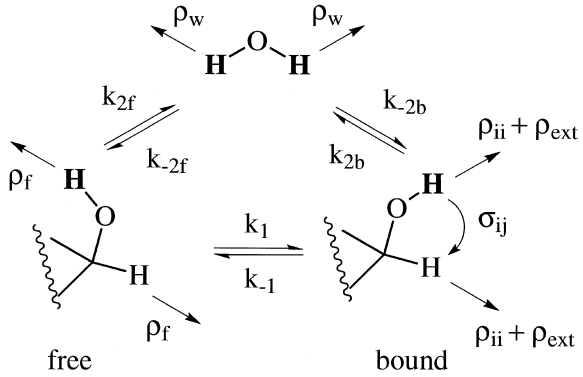


*Figure 6.* Kinetic scheme used to generate the dynamic matrix **D**. Exchangeable protons are shown in boldface type, and kinetic constants are described in the text.

the magnetization arises from exchangeable protons on the mannoside, namely the hydroxyl protons.

Given that mannoside hydroxyl protons mediate the magnetization transfer, it is possible that the two questions posed above could be addressed by a simple kinetic model. Such a model is displayed in Figure 6. This scheme models the interactions between five spins: a water proton, a mannoside ring proton in the bound and free states, and a mannoside hydroxyl proton in the bound and free states. The following chemical kinetic rate constants are included in the model: the pseudo-first order rate constant for the on-rate of mannoside binding ($k_1$), the first order rate constant for the off-rate ($k_{-1}$), and the pseudo-first order rate constants for the forward and back water exchange rates of a hydroxyl proton in the free ($k_{2f}$, $k_{-2f}$) and bound ($k_{2b}$, $k_{-2b}$) states. In addition to these rate constants, rate constants for longitudinal relaxation were included for each spin along with a rate constant for cross-relaxation between a hydroxyl and ring proton in the bound state. To simulate the loss of magnetization in the bound state from spin diffusion to MBP protons, a leakage rate constant, $\rho_{ext}$, was added to the longitudinal relaxation rate constants of the bound ring and hydroxyl protons. The cross-relaxation rate constant in the free state was assumed to be zero, as was the rate constant for direct cross-relaxation between water protons and ring protons.

This model was used to simulate magnetization transfer using generalized dynamic matrices (Lee and Krishna, 1992; Moseley et al., 1995). Briefly, a dynamic matrix **D** is constructed as the sum, **R** + **K**, of matrices containing the relaxation and chemical rate constants. Each matrix contains submatrices describing a given molecular species in the model. Peak intensities may then be calculated by diagonalizing the matrix **D** and using its matrix exponential. However, the generalized chemical kinetic matrix **K** is often asymmetric, causing **D** to be asymmetric. To avoid diagonalizing an asymmetric matrix, Moseley and coworkers demonstrated that a transformation matrix **S** can be easily constructed which can symmetrize **D**. Matrix **D** can then be diagonalized by a standard transformation **T** to yield the matrix Λ:

$$\Lambda = \mathbf{T}^{-1}\mathbf{S}^{-1}\mathbf{DST} \tag{1}$$

The expression for peak intensities, $\mathbf{I}(\tau)$, can then be written as follows:

$$\mathbf{I}(\tau) = \mathbf{ST}\exp(-\Lambda\tau)\mathbf{T}^{-1}\mathbf{S}^{-1}[\mathbf{I}(0) - \mathbf{I}(\infty)] + \mathbf{I}(\infty) \tag{2}$$

where $\mathbf{I}(0)$, $\mathbf{I}(\tau)$, and $\mathbf{I}(\infty)$ are square matrices of magnetizations of each spin at the beginning of the mixing time, after a mixing time τ, and at equilibrium, respectively. In our specific application, we assumed that the hydroxyl protons are in fast exchange with water and are simultaneously inverted with water by the initial selective pulse. The analysis of the experiment thus proceeded essentially as a one-dimensional transient cross-relaxation experiment in which the water/hydroxyl spins were selectively inverted and the

buildup of magnetization was observed on the ring protons. The dynamic matrix $\mathbf{D} = \mathbf{R} + \mathbf{K}$ was a 5 × 5 matrix where **K** included the six aforementioned chemical rate constants. **R** included longitudinal relaxation rate constants, $\rho_f$ and $\rho_w$, as diagonal elements for the free ligand spins and water, and both longitudinal and cross-relaxation rate constants, $\rho_{ii}$ and $\sigma_{ij}$, for the bound ligand spins. These latter spin relaxation rate constants were computed conventionally as linear combinations of zero-, single-, and double-quantum transition probabilities of a two-spin system undergoing dipolar relaxation (Macura and Ernst, 1980):

$$\rho_{ii} = W_0^{ij} + W_{1i}^{ij} + W_2^{ij}; \sigma_{ij} = W_2^{ij} - W_0^{ij} \qquad (3)$$

In addition, the leakage rate constant $\rho_{ext}$ was added to the diagonal elements of the bound ring and hydroxyl protons to account for spin diffusion.

Input parameter values for the model were obtained either from experiment or from the literature. Values of $\rho_w$ and $\rho_f$ were obtained from standard inversion recovery experiments. Maximum values for $k_1$ and $k_{-1}$ were calculated from the known dissociation constant with the assumption of a diffusion-limited second-order rate constant for ligand binding ($k_{on} \sim 10^8\ M^{-1}s^{-1}$). Minimum values were calculated from the observed line broadening due to exchange ($\ll$ 10 Hz) and the chemical shift changes ($\sim$ 100 Hz). These calculations indicate that $k_{-1} > 1000\ s^{-1}$ and that $k_1 > 290\ s^{-1}$ (Reuben and Fiat, 1969). The two pairs of water exchange rate constants ($k_{2f}$, $k_{-2f}$; $k_{2b}$, $k_{-2b}$) can be related as follows:

$$k_{2f}[FOH] = k_{-2f}[HOH] \qquad (4a)$$
$$k_{2b}[BOH] = k_{-2b}[HOH] \qquad (4b)$$

where [FOH] and [BOH] represent the equilibrium concentrations of free and bound hydroxyl protons, respectively, and [HOH] represents the concentration of water protons. Since [FOH] and [BOH] can be calculated from the binding constant and the concentration of water protons is known (110 M), $k_{-2f}$ and $k_{-2b}$ can be obtained directly from the values of $k_{2f}$ and $k_{2b}$, which are the two remaining independent parameters. While the value of $k_{2f}$ must be at least $100\ s^{-1}$ since no hydroxyl signals are observed for the free sugar, an approximate value of $1000\ s^{-1}$ was used based on hydroxyl exchange data acquired at low temperature on sucrose (Adams and Lerner, 1992) and on serine and threonine at temperatures up to 36 °C (Liepinsh and Otting, 1996). The remaining undefined parameters are $k_{2b}$, $\rho_{ii}$, $\sigma_{ij}$, and $\rho_{ext}$. While the values of these parameters are unknown in general, reasonable ranges for these values can be obtained from the well-known geometry of the mannoside ring and from the literature. The spin relaxation rate constants $\rho_{ii}$ and $\sigma_{ij}$ are calculated using Equation (3) for proton–proton dipolar relaxation, and are thus dictated by the choice of two parameters, the rotational correlation time, $\tau_c$, of MBP and the hydroxyl proton-ring proton internuclear distance, *r*. An estimate for $\tau_c$ of 25 ns at 35 °C was obtained by extrapolating literature values for other proteins (Campbell and Sykes, 1993; Tjandra et al., 1996). Thus, both $\rho_{ii}$ and $\sigma_{ij}$ can be represented by the single parameter, *r*. Using molecular modeling, the range of values of *r* for a hydroxyl group and its geminal ring proton was found to be 2.06–2.84 Å, with the three stable gauche rotamers yielding *r* values of 2.28, 2.28, and 2.84 Å, respectively. Two limiting values of $\rho_{ext}$ were selected: first, the case where no spin diffusion occurs ($\rho_{ext} = 0$), and second, the case where spin diffusion is extensive, and $\rho_{ext} \approx 1/T_2$ of MBP. An approximate value for the MBP $T_2$ of 10 ms was obtained from experimental free induction decays. The value of $k_{2b}$ is more difficult to restrict, since one can envision scenarios in which water exchange is either inhibited or catalyzed within a protein binding site. We thus left the value of $k_{2b}$ unrestricted.

First we address the question of why the cross-relaxation buildup rates at the various ring protons are different. In general, we would expect that the rate of signal buildup would be determined by the rate-limiting step in the magnetization transfer pathway. It is clear from Figure 6 that there are two pathways that are parallel up to the point of bound ligand by which water magnetization can transfer to ring proton magnetization: first, water protons may exchange with hydroxyl protons on the free mannoside, followed by ligand binding, followed by cross-relaxation; and second, water protons may exchange with hydroxyl protons on the bound mannoside, followed by cross-relaxation. Both of these pathways conclude with loss of magnetization by spin diffusion, governed by $\rho_{ext}$. Given the above arguments, a maximum value of $\sigma_{ij}$ may be calculated from the minimum *r* value of the three stable hydroxyl rotamers and from the value of $\tau_c$. The resulting value of $\sigma_{ij}$ is $10\ s^{-1}$, yielding a rate of $10[BOH]\ Ms^{-1}$. For the first pathway, the prior successive processes are governed by $k_{-2f}$ and $k_1$. At equilibrium these rates are

$$k_{-2f}[HOH] = k_{2f}[FOH] \approx 1000[FOH]\ Ms^{-1} \qquad (5)$$

and

$$k_1[FOH] > 290[FOH]\,Ms^{-1} \quad (6)$$

Since [FOH] $\approx$ 2[BOH], we thus expect cross-relaxation to be rate-limiting. Considering the second pathway, the initial step occurs at a rate of $k_{-2b}[HOH] = k_{2b}[BOH]$, which is governed by $k_{2b}$. While we do not know this rate constant, it is easily seen that its value is irrelevant. If $k_{2b}$ is faster than $k_{2f}$, $\sigma_{ij}$ will remain rate-limiting. If $k_{2b}$ is slower than $k_{2f}$, the second pathway will be unable to compete with the first, and thus the size of $k_{2f}$ versus $\sigma_{ij}$ will still determine the rate-limiting step. Thus, the buildup rates should be largely determined by $\sigma_{ij}$, or at a constant $\tau_c$, by *r*. Figure 7 displays a series of curves generated by the proposed model for various values of *r* when $\rho_{ext} = 40\ s^{-1}$. As one might anticipate, the initial buildup rates are strongly dependent on *r*, while $\rho_{ext}$ determines the decay of signal at long mixing times.

Concerning the explanation for the apparently enhanced intensities of the water cross peaks relative to the intrasugar cross peaks, we chose to use the intramolecular cross peaks between H6 and H6′ observed in the 2D $^{13}$C-filtered NOESY spectra (see Figure 2) as a representative example of a case where water exchange is not involved. We thus sought those model parameters that would yield curves that are most consistent with the intensities of the exocyclic cross peaks in spectra acquired with mixing times of 50 and 100 ms. The distance between H6 and H6′ is constant and well known (1.82 Å), yielding a fixed value of $\sigma_{ij}$. Thus, $\rho_{ext}$ is the only remaining parameter which should dictate the shape of the buildup curves. The proposed model yielded curves that were consistent with data for values of $\rho_{ext}$ of approximately $50\ s^{-1}$ at 25 °C. One such curve is displayed in bold in Figure 8, along with a family of curves representing a ring/hydroxyl proton pair in a stable rotamer ($r$ = 2.28 Å) for various rates of water exchange. Other parameters were set as detailed in the legend to Figure 8. The family of curves clearly demonstrates that water exchange can enhance the buildup of magnetization by more than a factor of two. The enhancement increases with the exchange rate (curves g $\rightarrow$ a), but it becomes essentially constant when the exchange rate is higher than $\sim 500\ s^{-1}$ (curves a and b). As the figure shows, the intensities still remain below that of the H6-H6′ cross peaks at mixing times less than $\sim$ 100 ms, in contrast to the spectrum which shows that at a mixing time of 50 ms the volumes of the water cross peaks are approximately 50% larger than those of the H6-H6′ cross peaks.

The model presented in Figure 6 is therefore able to explain the differences in buildup rates at various ring protons, and is able to explain partially the enhancement of signal due to water exchange. It is, however, likely that the model remains too simple. The proposed model only considers cross-relaxation between a given hydroxyl proton and its geminal ring proton. However, the distance between a given hydroxyl proton and its vicinal ring proton can range from approximately 2.1 to 3.5 Å, making such vicinal cross-relaxation competitive with geminal cross-relaxation for many orientations. Therefore, *simultaneous* cross-relaxation between a hydroxyl proton and both its geminal and vicinal ring protons is quite likely. Indeed, the fact that any magnetization is transferred to H5 in the water-selective 2D NOESY-HSQC (see Figure 4) indicates that cross-relaxation with vicinal hydroxyls does occur, since H5 has no geminal hydroxyl group. These additional interactions with protons resonating at the water band will raise the amplitude of the water cross peaks, and when these processes are added to the model, the modified model should then provide an explanation for the signal enhancement due to water exchange. Incorporating cross-relaxation between a ring proton and multiple hydroxyl protons into the kinetic model is straightforward, since the individual cross-relaxation rate constants can be assumed to be independent and to sum to an effective larger relaxation rate constant.

*Development of a structural model*

Having found a model that is likely to answer our two initial questions, it is useful to ask if the model can provide insights into the nature of ligand binding and perhaps the geometry of the bound ligand. Given fast ligand binding kinetics and fast water exchange, the modified model will still predict that the initial rates of the cross-relaxation buildup curves should be largely dependent on $\sigma_{ij}$. However, $\sigma_{ij}$ is no longer a simple function of a single value *r*, but is a function of multiple distances, $r_{ij}$, between hydroxyl protons, $OH_i$, and a given ring proton, $H_j$. If the rates of exchange are slow compared to the overall molecular tumbling (25 ns), a net cross-relaxation rate constant can be defined:

$$\sigma_j = \sum_i \sigma_{ij} \propto \sum_i \frac{1}{r_{ij}^6} = \zeta_j \quad (7)$$

The task now becomes one of determining a set of viable structural models for the mannoside which can

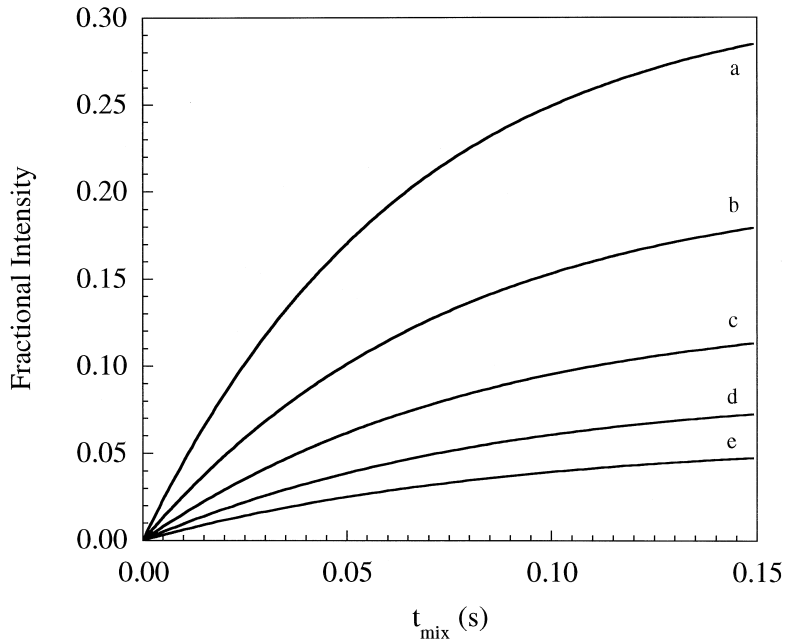


*Figure 7.* Theoretical curves generated by the kinetic model described in the text. Data are plotted as the fractional intensity of total ring proton magnetization (free + bound) at $t_{mix} = 0$. Curves a–e represent predicted signal intensities for a ring proton resulting from cross-relaxation with its geminal hydroxyl at various values of *r*, which are respectively 2.0, 2.2, 2.4, 2.6, and 2.8 Å. In curves a–e, $k_{2f} = k_{2b} = 1000\ s^{-1}$. The value of $\rho_{ext}$ was set to 40 $s^{-1}$ to account for the fact that the water-selective data were acquired at 35 °C. Other parameters were held fixed at the following values: $k_1 = 8.0 \times 10^4\ s^{-1}$, $k_{-1} = 2.8 \times 10^5\ s^{-1}$, $\rho_f = 1.5\ s^{-1}$, $\rho_w = 0.2\ s^{-1}$, $\rho_{ext} = 25$ ns.

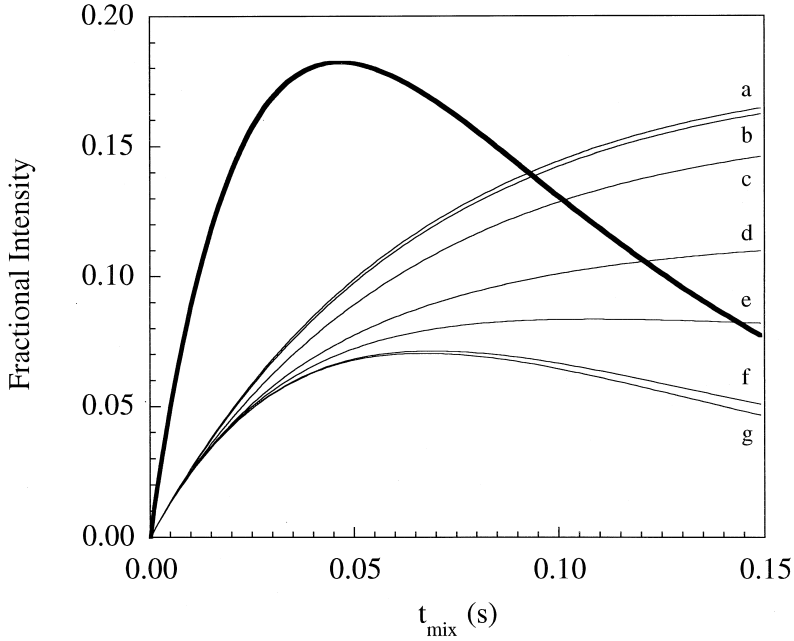


*Figure 8.* Theoretical curves generated by the kinetic model described in the text. Data are plotted as the fractional intensity of total ring proton magnetization (free + bound) at $t_{mix} = 0$. The curve in bold represents the buildup and decay of H6 signal intensity from cross-relaxation with H6′, with $r = 1.82$ Å and $k_{2f} = k_{2b} = 0\ s^{-1}$. The value of $\tau_c$ used was 32 ns to account for the fact that the H6-H6′ cross-relaxation data were collected at 25 °C. Curves a–g represent the predicted signal intensities for a ring proton resulting from cross-relaxation with its geminal hydroxyl at $r = 2.28$ Å for various values of $k_{2f} = k_{2b}$, which are respectively 1000, 500, 100, 25, 10, 1, and 0.1 $s^{-1}$. Other parameters for all curves were held fixed at the following values: $k_1 = 8.0 \times 10^4\ s^{-1}$, $k_{-1} = 2.8 \times 10^5\ s^{-1}$, $\rho_f = 1.5\ s^{-1}$, $\rho_w = 0.2\ s^{-1}$, $\rho_{ext} = 50\ s^{-1}$.

*Table 2.* Comparison of initial slopes of signal buildup data at various ring protons with calculated ζ values for preferred rotamers of hydroxyls 3 and 4

| Structure | OH3 | OH4 | H2 | H3 | H4 | H5 | $\epsilon$[a] |
|---|---|---|---|---|---|---|---|
| Exp. slopes | – | – | 0.117[b] | 0.101 | 0.109 | 0.0313 | – |
| I | ap | −sc[c] | 0.0710[d] | 0.0295 | 0.167 | 0.0242 | 4.35 |
| II | ap | ap | 0.0710 | 0.0965 | 0.119 | 0.0683 | 3.75 |
| III | −sc | −sc | 0.0938 | 0.0935 | 0.119 | 0.0241 | 1.65 |
| IV | −sc | ap | 0.0938 | 0.160 | 0.0704 | 0.0682 | 3.82 |

[a] Calculated as the root of the sum of the squared residuals of the six ratios between the four ζ values.
[b] Values in arbitrary units.
[c] Rotamer states are identified by ap (anti-periplanar) or −sc (−syn-clinal) based on the relative positions of the hydroxyl proton and geminal ring proton when looking down the O-C bond.
[d] Values of ζ in $Å^{-6}$.

*Table 3.* Distances between mannoside hydroxyl protons and nearby hydrogen bond acceptors on MBP

| Hydroxyl | Rotamer | Glu 193 O | Asn 205 N | Asn 187 N | Glu 185 O |
|---|---|---|---|---|---|
| OH3 | ap | – | – | 1.97[a] | 3.20 |
| OH3 | −sc | – | – | 2.78 | 1.68 |
| OH4 | ap | 3.37 | 2.02 | – | – |
| OH4 | −sc | 1.87 | 3.36 | – | – |

[a] Values in Å.

yield a set of $\zeta_j$ values consistent with experimental data.

We are aided in this structural analysis by the well-known geometry of the mannoside ring, which allows us to assume that the only structural variation in the ligand will be the rotation of the four hydroxyl groups about the C-O bonds, and the rotation of the exocyclic hydroxymethyl group about the C5-C6 bond. Moreover, we believe we can eliminate this hydroxymethyl group from consideration due to its local dynamics. Numerous studies on carbohydrates in free solution have uniformly determined that this group undergoes rapid torsional librations (McCain and Markley, 1987; Hajduk et al., 1993; Mäler et al., 1996). If one considers the model of the MBP binding site based on the crystal structure, one notes that the hydroxymethyl group is oriented away from the protein into free solvent, thus providing little hindrance to these motions. Since rapid internal motions of protein side chains can significantly reduce the rates of cross-relaxation involving these groups (Liepinsh and Otting, 1996), we expect the cross-relaxation rates involving the hydroxymethyl group to be reduced similarly. If the cross-relaxation rate from OH6 is reduced even by a factor of two, its contribution to magnetization transfer to H4 and H5 (the only two ring protons that OH6 can approach within 5 Å) becomes relatively insignificant compared to that from the remaining, more intimately packed hydroxyl groups. We thus focus on OH2, OH3, and OH4, considering only those structures consistent with the threefold rotational minima for these hydroxyls. We are then left with an ensemble of 27 possible structures.

The set of possible structures can be further reduced by examining the specific protein-sugar interactions allowed in the crystal structure. The resulting model proposes that the oxygens of OH3 and OH4 each form a coordination bond with the binding site calcium using one of their lone pairs. This model thus excludes hydroxyl rotamers which orient the oxygen lone pairs away from the binding site calcium. Turning to OH2, there are no specific interactions between this hydroxyl and the protein that can be inferred from the crystal structure. We will thus assume that the three stable rotamers of OH2 are equally populated. We are left with four possible structures based on the rotameric state of OH3 and OH4.

The calculated $\zeta_j$ values for these four structures are summarized in Table 2. For reference, the initial slopes of the experimental buildup curves are also provided. It is clear from these data that the rotamer combination that is most consistent with the experimental curves is structure III. This model is a significantly better match than any of the other three structures. At a minimum, an ensemble of rotamer states must be selected in which structure III is dominant.

As shown in Table 3, the two available rotamers for OH3 and OH4 position the hydroxyl protons within hydrogen bonding distance of different protein acceptor groups. Interestingly, structure III directs these protons toward one of the carboxylate oxygens of Glu 185 and Glu 193, respectively, which are the nearest hydrogen bond acceptors available to them. In addition, both of these rotamer states allow the second lone pair of each hydroxyl oxygen (the lone pair not involved in binding to the calcium) to serve as a hydrogen bond acceptor to one of the amide protons of a nearby asparagine side chain: Asn 187 in the case of OH3, and Asn 205 in the case of OH4. Such multiple hydrogen bonds are not possible in the other rotamer states. These considerations provoked Weis and co-workers to argue for precisely the hydroxyl rotamer states of structure III when they discussed their crystal structure of MBP complexed with a bound mannose-rich oligosaccharide (Weis et al., 1992). Thus, our magnetization transfer data and the model that explains it offer direct evidence for the specific placement of hydroxyl protons in the protein binding site.

Direct data on the placement of hydrogen bonding protons in a carbohydrate binding site of a protein are important in rationalizing the specificity of ligand binding. We have shown that at least under conditions where the ligand is in fast exchange between bound and free forms and where proton exchange with water is relatively fast, these data can be obtained from a combination of selective water inversion and ligand based $^{13}C$ filtering experiments. Given the increasing availability of isotopically labeled carbohydrates, the application of this methodology to other systems should be possible.

## Acknowledgements

This work was supported by an NIH grant, GM 33225, and by a Howard Hughes Medical Institute Predoctoral Fellowship to E.W.S. We thank Kurt Drickamer for providing the clone of MBP and Michael Andrec for assistance with implementation of the kinetic model and many helpful discussions.

## References

Adams, B. and Lerner, L. (1992) *J. Am. Chem. Soc.*, **114**, 4827–4829.
Adams, B. and Lerner, L.E. (1994) *Magn. Reson. Chem.*, **32**, 225–230.
Andrec, M., Hill, R.B. and Prestegard, J.H. (1995) *Protein Sci.*, **4**, 983–993.
Bevilacqua, M.P. (1993) *Annu. Rev. Immunol.*, **11**, 767–804.
Campbell, A.P. and Sykes, B.D. (1993) *Annu. Rev. Biophys. Biomol. Struct.*, **22**, 99–122.
Casu, B., Reggiani, M., Gallo, G.G. and Vigevani, A. (1966) *Tetrahedron*, **22**, 3061–3083.
Cavanagh, J., Fairbrother, W.J., Palmer, A.G.I., and Skelton, N.J. (1996) *Protein NMR Spectroscopy*, Academic Press, San Diego, CA.
Chang, C.Y., Sastry, K.N., Gillies, S.D., Ezekowitz, R.A.B. and Sheriff, S. (1994) *J. Mol. Biol.*, **241**, 125–127.
Clore, G.M. and Gronenborn, A.M. (1983) *J. Magn. Reson.*, **53**, 423–442.
Davis, A.L., Keeler, J., Laue, E.D. and Moskau, D. (1992) *J. Magn. Reson.*, **98**, 207–216.
Drickamer, K. (1989) *Biochem. Soc. Trans.*, **17**, 13–15.
Ferrier, R.J. and Prasad, N. (1968) *Chem. Commun.*, 476.
Fornstedt, N. and Porath, J. (1975) *FEBS Lett.*, **57**, 187–191.
Grzesiek, S. and Bax, A. (1993) *J. Biomol. NMR*, **3**, 627–638.
Hajduk, P.J., Horita, D.A. and Lerner, L.E. (1993) *J. Am. Chem. Soc.*, **115**, 9196–9201.
Hare, B.J., Sanders, C.R.I., McIntyre, S.E. and Prestegard, J.H. (1993) *Chem. Phys. Lipids*, **66**, 155–158.
Hoppe, H.-J. and Reid, K.B.M. (1994a) *Protein Sci.*, **3**, 1143–1158.
Hoppe, H.-J. and Reid, K.B.M. (1994b) *Structure*, **2**, 1129–1133.
Hounsell, E.F. (1995) *Prog. NMR Spectrosc.*, **27**, 445–474.
Iobst, S.T., Wormald, M.R., Weis, W.I., Dwek, R.A., and Drickamer, K. (1994) *J. Biol. Chem.*, **269**, 15505–15511.
John, B.K., Plant, D., Webb, P. and Hurd, R.E. (1992) *J. Magn. Reson.*, **98**, 200–206.
Kriwacki, R.W., Hill, R.B., Flanagan, J.M., Caradonna, J.P. and Prestegard, J.H. (1993) *J. Am. Chem. Soc.*, **115**, 8907–8911.
Lasky, L.A. (1992) *Science*, **258**, 964–969.
Lee, R.T., Ichikawa, Y., Fay, M., Drickamer, K., Shao, M.-C. and Lee, Y.C. (1991) *J. Biol. Chem.*, **266**, 4810–4815.
Lee, W. and Krishna, N.R. (1992) *J. Magn. Reson.*, **98**, 36–48.
LeRoux, P. (1988) In *Proc. Magn. Reson. Med., 7th Annu. Meeting*, (Eds, Raymond, A.E.), Academic Press, San Diego, CA, pp. 1049.
Liepinsh, E. and Otting, G. (1996) *Magn. Reson. Med.*, **35**, 30–42.
Macura, S. and Ernst, R.R. (1980) *Mol. Phys.*, **41**, 95–117.
Mäler, L., Widmalm, G. and Kowalewski, J. (1996) *J. Biomol. NMR*, **7**, 1–7.
McCain, D.C. and Markley, J.L. (1987) *J. Magn. Reson.*, **73**, 244–251.
Mori, S., Berg, J.M. and van Zijl, P.C.M. (1996) *J. Biomol. NMR*, **7**, 77–82.
Moseley, H.N.B., Curto, E.V. and Krishna, N.R. (1995) *J. Magn. Reson.*, **B108**, 243–261.
Muhandiram, D.R., Farrow, N.A., Xu, G.-Y., Smallcombe, S.H. and Kay, L.E. (1993) *J. Magn. Reson.*, **B102**, 317–321.

Opdenakker, G., Rudd, P.M., Ponting, C.P. and Dwek, R.A. (1993) *FASEB J.*, **7**, 1330–1337.
Otting, G., Liepinsh, E. and Wüthrich, K. (1991) *Science*, **254**, 974–980.
Poppe, L. and van Halbeek, H. (1991) *J. Am. Chem. Soc.*, **113**, 363–365.
Poppe, L. and van Halbeek, H. (1994) *Nat. Struct. Biol.*, **1**, 215–216.
Quiocho, F.A. (1989) *Pure Appl. Chem.*, **61**, 1293–1306.
Reuben, J. and Fiat, D. (1969) *J. Chem. Phys.*, **51**, 4918–4927.
Shaka, A.J., Barker, P.B. and Freeman, R. (1985) *J. Magn. Reson.*, **64**, 547–552.
Sheriff, S., Chang, C.Y. and Ezekowitz, R.A.B. (1994) *Nat. Struct. Biol.*, **1**, 789–794.
Shinnar, M., Eleff, S., Subramanian, H. and Leigh, J.S. (1989) *Magn. Reson. Med.*, **12**, 74–80.
Tjandra, N., Grzesiek, S. and Bax, A. (1996) *J. Am. Chem. Soc.*, **118**, 6264–6272.
Tolman, J.R., Chung, J. and Prestegard, J.H. (1992) *J. Magn. Reson.*, **98**, 462–467.
Weis, W.I., Crichlow, G.V., Murthy, H.M.K., Hendrickson, W.A. and Drickamer, K. (1991a) *J. Biol. Chem.*, **266**, 20678–20686.
Weis, W.I., Kahn, R., Fourme, R., Drickamer, K. and Hendrickson, W.A. (1991b) *Science*, **254**, 1608–1615.
Weis, W.I., Drickamer, K. and Hendrickson, W.A. (1992) *Nature*, **360**, 127–134.
Weis, W.I. and Drickamer, K. (1994) *Structure*, **2**, 1227–1240.
Wishart, D.S., Bigam, C.G., Yao, J., Abildgaard, F., Dyson, H.J., Oldfield, E., Markley, J.L. and Sykes, B.D. (1995) *J. Biomol. NMR*, **6**, 135–140.